A&A 408, 101–109 (2003)
DOI: 10.1051/0004-6361:20030893

Astronomy & Astrophysics

The narrow line region of Ark 564

M. Contini[1,3], A. Rodríguez-Ardila[2], and S. M. Viegas[1]

[1] Instituto de Astronomia, Geofísica e Ciências Atmosféricas, Rua do Matão 1226, CEP 05508-900, São Paulo, SP, Brazil
e-mail: viegas@astro.iag.usp.br
[2] Laboratório Nacional de Astrofísica, Rua dos Estados Unidos 154, Bairro das Nações, CEP 37500-000, Itajubá, MG, Brazil
e-mail: aardila@lna.br
[3] School of Physics and Astronomy, Tel-Aviv University, Ramat-Avit, Tel-Aviv 69978, Israel

Received 14 February 2003 / Accepted 5 June 2003

Abstract. The continuum and emission-line spectrum of the narrow-line Seyfert 1 galaxy Ark 564 is used to investigate, for the first time, the physical conditions and structure of its narrow line region (NLR). For this purpose, composite models, accounting for the coupled effect of photoionization and shocks, are employed. The emission-line spectrum of Ark 564, which ranges from the ultraviolet to the near-infrared, shows a rich forbidden line spectrum. Strong emphasis is given to the study of the coronal line region. The diversity of physical conditions deduced from the observations requires multi-cloud models to reproduce the observed lines and continuum. We find that a combination of high velocity (V_s = 1500 km s^{-1}) shock-dominated clouds as well as low velocity (V_s = 150 km s^{-1}) radiation-dominated clouds explains the coronal lines, while the optical low-ionization lines are mainly explained by shock-dominated clouds. The results for Ark 564 are compared with those obtained for other Seyfert galaxies previously analyzed such as NGC 5252, Circinus, NGC 4051 and NGC 4151. The model results for the ultraviolet and optical permitted lines suggest that the broad line region may contribute up to 80%, depending on the emission-line, being of about 30% for Hβ. The consistency of the multi-cloud model is checked by comparing the predicted and observed continuum, from radio to X-ray, and indicate that the dust-to-gas ratio in the clouds varies from 10^{-15} to 10^{-12}.

Key words. galaxies: Seyfert – galaxies: individual: Ark 564 – infrared: galaxies – line: formation

1. Introduction

Narrow-line Seyfert 1 galaxies (NLS1) are a peculiar group of active galactic nuclei (AGN) with extreme properties. Their permitted optical lines emitted by the broad line region (BLR) show full widths at half-maximum (*FWHM*) not exceeding 2000 km s^{-1}, the [O III]/Hβ ratio is less than 3, and the UV-optical spectrum is usually dominated by strong Fe II emission multiplets (Osterbrock & Pogge 1985). In the soft X-ray, NLS1 have generally much steeper continuum slopes and rapid variability (Boller et al. 1996). In addition, Leighly (1999) found that the hard X-ray photon index is significantly steeper in NLS1 compared with that of classical Seyfert 1 and that soft excess emission appears considerably more frequently in the former than in the later. Nowadays, the most accepted explanation for the above properties is that these objects have relatively low black-hole masses for their luminosity but high accretion rates (Boller et al. 1996). In fact, observational evidence obtained through reverberation mapping techniques points toward the presence of a black hole of smaller mass in NLS1 ($M_{\rm BH} \sim 10^{6-7}\ M_\odot$) than that of other broad-line AGN ($M_{\rm BH} \sim 10^{7-9}\ M_\odot$; Peterson & Wandel 2000) with similar luminosity.

While most efforts have been devoted to explain the extreme properties associated to the BLR in NLS1, very little has been said about the properties of the narrow line region (NLR) in these objects and how do they compare to that of other AGN, except for a few works reported in the literature (Goodrich 1989; Rodríguez-Ardila et al. 2000; Nagao et al. 2001; Rodríguez-Ardila et al. 2002). Given that the NLR is one of the fundamental ingredients of AGN, every effort to understand what NLS1 are must include a detailed investigation of the NLR at least for the following three reasons.

First, the NLR is the largest structure directly affected by the radiation from the central engine. Therefore, if the spectral energy distribution (SED) of the ionizing radiation flux is somehow different from that of classical Seyferts, the resulting ionization structure of the NLR gas should be different, as it is observed in some NLS1 (Rodríguez-Ardila et al. 2000).

Second, NLS1 are located at the extreme end of the anti-correlation between [O III] and Fe II (Boroson & Green 1992), namely, Fe II is strong in objects with weak [O III] emission and weak in those with strong [O III]. That inverse correlation suggests the existence of a physical mechanism which balances

Send offprint requests to: M. Contini,
e-mail: marcel@wise1.tau.ac.il

Fe II excitation against the illumination of the NLR. Although the nature of the Fe II is out of the scope of this paper, the study of the NLR in NLS1 may provide important clues to identify the parameter linking BLR and NLR excitation.

Third, the spectra of NLS1 usually display strong high ionization forbidden emission lines (also known as coronal lines) such as [Fe X] λ6374, [Fe XI] λ7892 and [Fe XIV] λ5303 (Penston et al. 1984; De Robertis & Osterbrock 1984). Up to now, it is not clear what the physical mechanisms involved in the production of these features are, but three possible scenarios have been suggested: *(i)* collisional ionization of gas with temperatures of $T_e \sim 10^6$ K (Oliva et al. 1994); *(ii)* photoionization by the central non-thermal continuum (Ferguson et al. 1997); and *(iii)* a combination of shocks and photoionization (Viegas-Aldrovandi & Contini 1989; Contini & Viegas 2001). Although these lines are common in most AGN, NLS1 appear as suitable candidates to investigate their origin because they are not severely blended with nearby broad features as in classical Seyfert 1 or diluted by stellar absorption features as in Seyfert 2.

The study of the NLR in NLS1 is not straightforward, however. Deblending the optical permitted lines in NLS1 is difficult because no transition between the narrow and broad components is observed. This shortcoming translates into large uncertainties in determining the fraction of Hα and Hβ that is emitted by the NLR, affecting in turn, the determination of the reddening of the NLR gas. The extinction correction should then relay on other indicators such as ratios of forbidden lines of the same ion, separated by a large wavelength interval, yet not always observed with the same instrumental setup.

For the above reasons, we have started a program to study, in a consistent way, the NLR of a selected sample of NLS1 galaxies with the aim of investigating the physical conditions and structure of that region, with particular emphasis in the origin of the coronal lines. To that purpose, composite models accounting for both the effects of photoionization by a central continuum source and shocks, created by collision of gas clouds with the intercloud medium, will be employed. The well-known NLS1 galaxy Arakelian 564 ($z = 0.0247$) is a suitable candidate to begin with. The strong coronal line spectrum observed by Rodríguez-Ardila et al. (2002, hereafter RVPP02) in the near-infrared region (NIR) as well as the optical measurements reported by Erkens et al. (1997, hereafter E97) on this source form one of the most complete set of lines available for modeling the NLR and studying the effects of shocks on line intensities in a NLS1. Following Moran (2000), Ark 564 exhibits an unresolved radio core and what appears to be a small scale ($\sim$1″) jet. This feature strengthens the hypothesis that shocks are at work. Moreover, it suggests that extended synchrotron radiation should be observed in the radio range.

Ark 564 has been extensively studied from radio to X-rays, allowing a consistent modeling of both the line and continuum emission. Among other reasons that turn this target interesting is that it is the brightest known NLS1 in the 2–10 keV band (Collier et al. 2001). The results of an intensive variability campaign on several wavelength bands show that the optical continuum is not significantly correlated with the X-rays (Shemmer et al. 2001). The ionization state of the gas, as described by Crenshaw et al. (2002), is relatively high. They found that at least 85% of the narrow emission-line flux comes from a region $\leq$95 pc from the nucleus and surrounded by a dust screen associated to a "lukewarm" absorber.

In Sect. 2 we describe the data set used to the study the NLR. A description of the modeling output and fitting to the line fluxes is given in Sect. 3. As a consistency check, the fit of the continuum emission SED is presented in Sect. 4. Discussion of results follows in Sect. 5 and Conclusions in Sect. 6.

2. The data

The NLR emission-line fluxes used in this work were primarily taken from E97 and RVPP02 for the optical (0.34–0.95 μm) and NIR (0.80–2.34 μm) lines, respectively. Both sets of data were taken at similar resolution and S/N. Although the slit width employed in the optical observations was larger than that of the NIR ones (1.5″ and 0.8″, respectively), the contamination introduced by the host galaxy or extended emission to the optical fluxes is negligible. In both cases, the authors report that most of the integrated signal came from the unresolved nuclear region and that the spectra were extracted from pixels centered on the maximum of the continuum emission. This is confirmed by comparing the flux of the [S III] 0.953 μm line, common in both spectra. E97 measured a value of $3.06 \pm 0.13 \times 10^{-14}$ erg s^{-1} cm^{-2}, in very good agreement with the value of $3.11 \pm 0.10 \times 10^{-14}$ erg s^{-1} cm^{-2} reported by RVPP02.

For reddening correction, we used the value of $E(B-V) = 0.09 \pm 0.03$ reported by E97. Although it is a bit lower than the $E(B-V) = 0.14 \pm 0.04$ reported by Crenshaw et al. (2002), they agree within errors. The former value was determined applying the method of Allen (1979) to the [S II] 0.4068 μm, 0.4076 μm, [S II] 0.6717 μm, 0.6731 μm, [O II] 0.3727 μm and [O II] 0.7330 μm line pairs, and so, most suitable to the NLR. Columns 2 and 5 of Table 1 list the extinction corrected line ratios relative to the total Hβ flux. In order to avoid the uncertainties introduced by the deblending of the observed permitted lines into the component emitted by the NLR and BLR, we decided to normalize the narrow line fluxes to that of [O III] 0.5007+0.4959 μm. The resulting values are reported in Cols. 3 and 6 of that same table.

3. Modeling the spectra

The main goal of this work is to model the NLR spectrum of the NLS1 galaxy Ark 564 using the fluxes of optical and NIR coronal lines (see Table 1) as major constraints. This ensures that important information about high ionization material (see Contini et al. 2002a) is taken into account. The data from Table 1 imply that gas clouds with very different physical conditions must coexist in the NLR of this object. This is reflected, e.g. in the large interval of critical densities (10^3–10^9 cm^{-3}) of the transitions and ionization potentials (up to 370 eV) of the ions involved in the production of the observed forbidden lines, or in the large range of line widths – a factor of 3 in *FWHM* (see Table 5 of RVPP02) measured in the line profiles. With this in mind, we have run a grid of models with parameters in

Table 1. Emission line ratios[1] for Ark 564, corrected for $E(B-V) = 0.09$.

Line	F_λ/Hβ	F_λ/[O III]	Line	F_λ/Hβ	F_λ/[O III]
[Ne V] λ3425	16.5 ± 0.9	13.9 ± 0.9	[Fe X] λ6374	7.10 ± 0.42	5.97 ± 0.41
[O II] λ3727	16.3 ± 0.7	13.7 ± 0.7	[N II] λ6548	0.673 ± 0.041	2.79 ± 0.19
[Fe V] λ3839	0.226 ± 0.028	0.19 ± 0.02	Hα^a	355.0 ± 14.7	298 ± 16
[Ne III] λ3868	9.75 ± 0.41	8.2 ± 0.4	[N II] λ6583	9.97 ± 0.44	8.30 ± 0.46
[S II] λ4068	1.96 ± 0.11	1.65 ± 0.11	He I λ6678^a	1.73 ± 0.13	1.46 ± 0.12
[S II] λ4076	0.482 ± 0.038	0.40 ± 0.03	[S II] λ6716	3.88 ± 0.32	3.26 ± 0.29
[O III] λ4363	4.89 ± 0.21	4.11 ± 0.22	[S II] λ6730	4.51 ± 0.20	3.79 ± 0.21
He II λ4686^a	14.8 ± 4.7	12.4 ± 3.9	[Ar V] λ7005	0.656 ± 0.061	0.55 ± 0.05
[Ar IV] λ4711	1.01 ± 0.09	0.85 ± 0.08	[Ar III] λ7135	1.69 ± 0.09	1.42 ± 0.09
Hβ^a	100.0	84.1	[Ar III] λ7751	0.538 ± 0.100	0.45 ± 0.09
[Fe VII] λ4893	0.573 ± 0.075	0.48 ± 0.06	[Fe XI] λ7891	8.31 ± 0.39	7.0 ± 0.40
[Fe VII] λ4988	0.573 ± 0.088	0.48 ± 0.08	[S III] λ9069	5.76 ± 0.26	4.80 ± 0.27
[O III] λ5007 + 4959	118.9 ± 4.0	100.0	[S III] λ9532	10.7 ± 0.5	9.00 ± 0.52
[Fe VII] λ5145	0.283 ± 0.023	0.23 ± 0.02	[C I] 0.985 μm	0.23 ± 0.07	0.19 ± 0.06
[Fe VI] λ5159	1.01 ± 0.09	0.85 ± 0.08	[S VIII] 0.991 μm	1.75 ± 0.13	1.47 ± 0.12
[N I] λ5199	2.04 ± 0.12	1.72 ± 0.12	[Fe XIII] 1.074 μm	2.88 ± 0.55	2.42 ± 0.47
[Fe VI] λ5335	0.697 ± 0.097	0.59 ± 0.08	[S IX] 1.252 μm	1.99 ± 0.19	1.60 ± 0.16
[Fe VII] λ5721	2.31 ± 0.15	1.94 ± 0.14	[Fe II] 1.257 μm	0.97 ± 0.16	0.82 ± 0.14
He I λ5875^a	9.92 ± 0.52	8.34 ± 0.52	[Si X] 1.430 μm	4.55 ± 0.32	3.83 ± 0.30
[Fe VII] λ6087	3.64 ± 0.19	3.06 ± 0.19	[Si VI] 1.963 μm	1.89 ± 0.35	1.59 ± 0.30
[O I] λ6300	5.29 ± 0.23	4.45 ± 0.24	[Ca VIII] 2.321 μm	0.82 ± 0.26	0.69 ± 0.22

[1] Fluxes in the optical region, up to 8000 Å, were taken from E97. NIR lines, from 9000 Å and longward were taken from RVPP02.
[a] Permitted line with contribution from the BLR.

the range suitable to the NLR of AGN and selected the models that best matches at least some of the observed line ratios. The grid was based on Contini & Viegas (2001). The results are obtained by the SUMA code (Viegas & Contini 1994) which, besides the line and continuum spectra emitted by the gas, also calculates re-radiation by dust.

Several multi-cloud models, obtained from a weighted average of single clouds models, were calculated and compared with the observed data. For each multi-cloud model, higher weights were assigned to single-cloud models matching the largest number of line ratios. Using this approach, we selected two final models that emerged as the best solutions. In the following sections they will be analyzed in detail to determine which one best represents the NLR state of Ark 564.

3.1. The models

The general model assumes gaseous, dusty clouds, which move outwards from the active center (AC) and emit the line and continuum spectra. A shock front forms on the outer edge of the clouds, while the inner edge is reached by the radiation from the AC.

The input parameters are: the radiation flux intensity, $F_{\rm H}$ (in photons cm^{-2} s^{-1} eV^{-1} at 1 Ryd), the spectral index, α (=−1.5), the shock velocity, $V_{\rm s}$, the preshock density, n_0, the preshock magnetic field, B_0 (=10^{-4} Gauss), the dust-to-gas ratio by number, d/g, and the geometrical thickness, D, of the emitting clouds. Cosmic relative abundances (Allen 1973) are adopted. In radiation dominated (RD) clouds the effect of the flux from the AC prevails on the shock. In shock dominated (SD) clouds the flux is absent ($F_{\rm H} = 0$).

Notice that photoionization models with spectral index $\alpha = -2$ were adopted by Rodríguez-Ardila et al. (2000) in order to explain the low [O III]/Hβ line ratio observed in the NLS1 galaxies. The observations required both matter-bounded and ionization-bound clouds. However no attempt was made to fit coronal lines or other emission lines in wavelength ranges other than the optical one. The presence of a non-negligible velocity field, indicated by the *FWHM* of the emission-lines, suggests that composite models, accounting for shock and photoionization, and also providing regions of high and low density gas, are probably more appropriate to model the emission-line spectra of NLS1 galaxies.

Investigating the optical and UV properties of NLS1 galaxies, Constantin & Shields (2003) suggest a spectral index of −1.34 in the UV–blue continuum. On the other hand, *ROSAT* data show that the X-rays spectrum shows a power index steep and equal to −2.4 (Boller et al. 1996), while ASCA data, corresponding to a different energy range and used to analyze the X-rays variability, indicate a power index of the order

of −1.3. Analyzing the optical spectrum of Ark 564, Crenshaw et al. (2002) assume that the continuum of Ark 564 consists of power-laws with index −1.0 for energies less than 13.6 eV, −1.07 for 13.6 eV ≤ E ≤ 0.5 keV, and −1.6 for E > 0.5 keV (consistent with Turner et al. 2001). Therefore, at least from the observational point of view, there is no strong reason to adopt a power index steeper than −1.6.

Here we adopt a UV – X-rays power index $\alpha = -1.5$ for all the models, recalling that the shocked zone also contributes to the emission-line intensities, so that our results are less dependent on the shape of the ionizing radiation. As shown in the next sections, our models with $\alpha = -1.5$ provide a good fit to the observed emission-line spectrum in a large range of wavelengths.

In order to account for the constraints imposed by the observations (line widths, densities, etc.), the models selected from the grid show a large range of shock velocities (V_s = 100−1500 km s^{-1}) and preshock densities (n_0 = 100−700 cm^{-3}), as is shown in Table 2. Notice that the shock velocities in the models lead to temperatures in the post shock region between 1.5×10^5 K (V_s = 100 km s^{-1}) and 3×10^7 K (V_s = 1500 km s^{-1}), in agreement with the average temperature derived by E97 from the [Fe VII] lines for the region producing the coronal lines. An overview of the values for the initial conditions adopted for each of the 14 individual cloud models are listed in the first six entries of Table 2. Notice that the values *wr* correspond to the model relative weight. Thus, in order to obtain the fraction of the Hβ luminosity emitted by a given cloud, the relative weight should be multiplied by the corresponding Hβ value listed in Table 2 and normalized by the sum over all clouds.

The cloud geometrical thickness D was chosen between 3 and 10 pc, but some models represent filaments with D < 1 pc. These filaments are created by fragmentation of matter in a turbulent regime in the presence of shocks. Such clouds must be present in order to emit strong [Fe XI] consistent with weak [C I] lines. The clouds emitting strong Fe coronal lines are matter-bounded, so they are mostly composed of highly ionized gas at high temperature. In a search for variations of [Fe VII] and [Fe X] in high ionization Seyfert galaxies, Veilleux (1988) claims that neither [Fe X] nor [Fe VII] in Ark 564 show any significant variations between 1977 and 1988. Considering that time variations are related to D/V_s (the time in which the shock crosses a filament), a minimum time of 25 years would be needed to detect any variability on the line flux emitted by clouds of model m14 (see Table 2). This time would be much higher for other clouds (see the values of D/V_s), in perfect agreement with Veilleux's results.

The flux intensities range from 0 in SD models to $F_H = 5 \times 10^{12}$ photons cm^{-2} s^{-1} eV^{-1} at 1 Ryd in RD models. The luminosity of Ark 564 at 1 Ryd, $L = 7 \times 10^{43}$ erg s^{-1} (Romano et al. 2002), constraints the models. Actually, the luminosity at 1 Ryd corresponding to the maximum $F_H = 5 \times 10^{12}$ photons cm^{-2} s^{-1} eV^{-1} is 4.5×10^{44} erg s^{-1}, assuming full coverage of the source.

The main criterion adopted for selecting the final multi-cloud models is that the ratio of calculated results to the data is within a factor of ∼2. However, given that the clouds are distributed over a large volume of space, subjected to a variety of physical conditions, some line ratios may show slightly larger discrepancies. The single-cloud models which lead to the best two fitting multi-cloud models are presented in Table 2 and labeled M1 and M2. The resulting line ratios normalized to [O III] $\lambda\lambda$5007+4959 are compared with the observed ratios in Table 3.

The multi-cloud model M1 shows that [O III] is overpredicted by a factor of ∼1.5 (compare the resulting ratio for Hα) and [Fe X]/[Fe XI] is higher than observed by a factor of >2. Notice, however, that the observed lines (E97, RVPP02) show very complex line profiles, which could be an indication that more single-cloud components should be included provided they do not change significantly the overall spectrum emitted by the cloud combination. However, in order to include new components, additional constraints coming from the line profiles should be accounted for, which is out of the scope of this paper. Moreover, model M1 gives [N II] and [S II] values higher than observed. Since N and S are not the main gas coolants, this problem could be solved by changing the adopted abundances of these two elements without affecting the results for other lines.

On the other hand, model M2 shows a better agreement with the observed [Fe X]/[Fe XI] ratio (<3), even if the [Fe XI]/[O III] ratio is underpredicted, as well as [O I]/[O III], while the calculated He II/[O III] ratio is high. In addition, [N II] and [S II] ratios are too low in this model, which would be improved using a higher abundance for N and S.

Both models M1 and M2 underpredict the [N I]/[O III] ratio. Notice that the [N I] line is usually weak because the critical density for collisional deexcitation is very low (∼1000 cm^{-3}) and the volume transition zone of the clouds is usually very low or inexistent.

Apart for the above discrepancies, it is clear from the data of Table 3 that model M1 leads to a better agreement than M2 for a larger number of lines. But before we can definitively choose either of the two models as the one that better represents the NLR state of Ark 564, further constraints must be applied.

3.2. Relative contribution to the lines from different clouds – weights and line widths

The relative weights adopted to sum up the single-cloud models, *wr*, are given in Table 2. The relative contribution (in per cent) of each cloud to the total predicted line flux is also listed in Table 2 for the multi-cloud models M1 and M2.

The physical conditions of the gas in each cloud are represented by the ensemble of the input parameters of the corresponding model. In composite models, the shock velocity and the flux from the AC are fundamental. Although the shock velocity does not correspond exactly to the velocity of the gas, it can be used to discuss the *FWHM* of the lines presented by RVPP02 in their Table 5. Clearly, all the line profiles show some substructure, confirming that many different conditions contribute to the different lines. Particularly, the *FWHM* are all >300 km s^{-1}. This is confirmed by our modeling,

Table 2. Single-cloud models.

	m1	m2	m3	m4	m5	m6	m7	m8	m9	m10	m11	m12	m13	m14
V_s[1]	100	100	100	100	150	150	150	300	500	500	500	500	1000.	1500
n_0[2]	100	100	100	100	30	100	600	100	100	100	700	700	1000	300
F_H[3]	1.(9)	1.(10)	1.(11)	7.(11)	–	1.(12)	3.(12)	–	1.(10)	5.(12)	–	1.(11)	5.(12)	–
D[4]	1.	3.	3.	3.	0.003	0.01	0.003	3.	3.	3.	3.	1.	0.1	3.85(−2)
Hβ[6]	1.4(−2)	1.0(−1)	4.6(−1)	6.1(−1)1	1.6(−5)	3.3(−3)	3.7(−1)7	1.8(−4)	1.4(−3)	2.49(+1)	1.0(−2)	8.7(+3)	1.3(−2)	4.5(−2)
Model M1:														
wr	4.7(−4)	1.9(−4)	0.0	2.4(−5)	9.5(−1)	4.7(−4)	9.5(−5)	0.0	3.8(−4)	1.9(−7)	1.3(−4)	2.(−8)	4.7(−2)	1.1(−4)
d/g[5]	10.	10.	1.	500.	1.	1.	1.	10.	1000.	10.	1.	800.	–	–
%([Fe VII])	–	–	–	38.	21.	–	22.	–	0.7	9.	2.3	–	–	6.5
%([Fe X])	–	–	–	5.4	–	0.5	21.	–	–	1.	1.4	–	1.4	69.
%([Fe XI])	–	–	–	8.6	–	2.3	28.	–	–	1.5	0.9	–	8.2	50.
%([Fe XIII])	–	–	–	11.	–	18.	11.	–	0.5	1.4	1.8	–	2.8	53.
%([C I])	–	–	–	–	28.	–	–	–	34.	–	38.	–	–	–
%([S III])	4.	15.	–	0.9	31.	–	–	–	–	–	–	47.	–	–
%([S VIII])	–	–	–	11.	–	0.6	58.	–	–	1.9	0.9	–	–	27.
%([S IX])	–	–	–	6.7	–	1.7	23.	–	–	1.2	1.2	–	–	66.
%([Si VI])	–	–	–	40.	15.	–	29.	–	–	11.	0.9	2.1	–	1.2
%([Si X])	–	–	–	5.3	–	12.	20.	–	–	1.1	0.9	–	4.1	56.
%([O I])	23.	57.	–	–	12.	–	–	–	1.	–	6.6	–	–	–
%([O II])	13.	19.	–	–	65.	–	–	–	1.2	–	1.1	1.1	–	–
%([O III])	1.2	11.	–	36.	34.	–	2.3	–	–	2.6	0.7	12.	–	–
%([Ne III])	2.8	11.	–	21.	45.	–	0.8	–	–	16.	1.5	1.1	–	–
%([Ne V])	–	–	–	12.	22.	0.8	62.	–	–	23.	0.5	–	–	–
Model M2:														
wr	0.0	2.4(−4)	1.6(−5)	1.6(−4)	0.0	4.0(−2)	1.2(−3)	1.6(−1)	0.0	1.2(−5)	3.2(−3)	7.0(−7)	7.9(−1)	3.(−4)
%([Fe VII])	–	–	–	19.	–	–	20.	13.	–	42.	4.	–	–	1.4
%([Fe X])	–	–	–	5.3	–	6.2	39.	3.8	–	9.1	4.8	–	3.5	28.
%([Fe XI])	–	–	–	5.7	–	20.	35.	0.7	–	9.2	2.2	–	14.	14.
%([Fe XIII])	–	–	–	3.6	–	73.	7.	–	–	4.3	2.1	–	2.3	7.2
%([C I])	–	–	–	–	–	–	–	58.	–	–	42.	–	–	–
%([S III])	–	1.1	0.5	–	–	–	–	2.	–	0.8	0.5	95.	–	–
%([S VIII])	–	–	–	6.7	–	4.7	66.	3.1	–	11.	1.9	–	–	6.9
%([S IX])	–	–	–	5.7	–	18.	37.	3.3	–	9.3	3.7	–	–	23.
%([Si VI])	–	–	–	18.	–	–	24.	4.8	–	47.	1.4	4.9	–	–
%([Si X])	–	–	–	2.2	–	63.	15.	0.7	–	4.2	1.3	-	4.2	9.6
%([O I])	–	26.	4.7	–	–	–	–	11.	–	–	57.	0.8	–	–
%([O II])	–	3.8	0.6	–	–	–	–	85.	–	–	4.	6.2	–	–
%([O III])	–	1.5	1.3	25.	–	–	3.	5.	–	17.	1.7	45.	–	–
%([Ne III])	–	1.1	0.7	11.	–	–	0.8	6.1	–	75.	2.6	3.	–	–
%([Ne V])	–	–	–	7.	–	6.1	69.	3.8	–	13.	1.1	–	–	–

Column 1: lines 1–4 show the input parameters, followed by the Hβ calculated absolute flux for each model and then the output for the multi-cloud model M1 (relative weights wr, dust-to-gas ratios and percent contribution of each model to each line); the same for the multi-cloud model M2 appears in the last lines of the table. The d/g results come from the SED which is modeled only for the selected model M1.
Columns 2–15: the output of single model predictions.
[1] In km s^{-1}.
[2] In cm^{-3}.
[3] In photons cm^{-2} s^{-1} eV^{-1} at 1 Ryd.
[4] In 10^{19} cm.
[5] In 10^{-15}.
[6] In erg cm^{-2} s^{-1}.

Table 3. Multi-cloud model results.

Line	$(I_\lambda/[\mathrm{O\,III}])_{\mathrm{obs}}$	$(I_\lambda/[\mathrm{O\,III}])_{\mathrm{M1}}$	$(I_\lambda/[\mathrm{O\,III}])_{\mathrm{M2}}$	RM1[1]	RM2[1]	RHβ1[2]	RHβ2[2]
[Ne V] λ3425	14.0	25.0	29.0	1.77	2.10	2.32	1.33
[O II] λ3727	13.7	15	10	1.1	0.72	1.4	0.5
[Ne III] λ3868	8.2	7.0	9.6	0.84	1.17	1.1	0.74
[S II] λ4068+	2.0	1.7	1.4	0.84	0.67	1.1	0.42
[O III] λ4363	4.0	3.9	1.7	0.94	0.41	1.24	0.23
He II λ4686	12.0	22.0	40.0	1.80	3.19	2.38	2.0
[Ar IV] λ4711	0.9	1.7	1.8	2.0	2.2	2.7	1.4
[Fe VII] λ4988	1.0	1.8	2.5	1.8	2.58	2.4	1.6
[O III] λ5007	100	100	100	1.0	1.0	1.3	0.63
[N I] λ5199	1.7	0.5	0.1	0.26	0.06	0.34	0.04
[Fe VI] λ5335	0.6	1.1	0.8	1.87	1.46	2.5	0.94
He I λ5875	8.3	2.7	8.2	0.32	1.0	0.42	0.62
[Fe VII] λ6087	3.0	2.8	4.0	0.93	1.3	1.23	0.84
[O I] λ6300	4.4	4.5	1.3	1.01	0.30	1.33	0.20
[Fe X] λ6374	6.0	6.0	4.4	1.0	0.74	1.36	0.47
[N II] λ6548+	9.0	21.0	7.2	2.3	0.8	3.0	0.50
Hα	299	180	370	0.60	1.25	0.78	0.78
[S II] λ6716	3.3	11	1.8	3.28	0.56	4.3	0.34
[S II] λ6730	3.8	9.0	2.2	2.4	0.6	3.2	0.37
[Ar III] λ7751	1.9	2.0	3.8	1.07	1.98	1.4	1.25
[Fe XI] λ7891	7.0	2.0	2.2	0.3	0.32	0.4	0.20
[S III] λ9069+	14.0	10.0	19.0	0.71	1.36	0.94	0.86
[C I] 0.985 μm	0.19	0.20	0.45	1.01	2.5	1.33	1.5
[S VIII] 0.991 μm	1.5	1.7	2.0	1.18	1.4	1.55	0.87
[Fe XIII] 1.074 μm	2.4	2.3	5.0	0.96	2.0	1.3	1.3
[S IX] 1.252 μm	1.7	0.9	0.7	0.52	0.43	0.68	0.27
[Si X] 1.430 μm	4.0	2.0	3.7	0.56	1.0	0.74	0.62
[Si VI] 1.963 μm	1.6	1.2	1.9	0.76	1.2	1.0	0.76
[O III]/Hβ	1.19	1.56	0.75	–	–	–	–
Hα/Hβ	2.99	2.77	2.76	–	–	–	–

[1] RM1 and RM2 stand for the ratio $(I_\lambda/[\mathrm{O\,III}])_{\mathrm{calc}}/(I_\lambda/[\mathrm{O\,III}])_{\mathrm{obs}}$ for M1 and M2, respectively.
[2] RHβ1 and RHβ2 stand for the ratio $(I_\lambda/\mathrm{H}\beta)_{\mathrm{calc}}/(I_\lambda/\mathrm{H}\beta)_{\mathrm{obs}}$ for M1 and M2, respectively.

which shows (see Table 2) that all the coronal lines have strong contributions from clouds with $V_s \geq 300$ km s^{-1}.

As an example, the [S III] line is mainly produced by clouds with $V_s = 500$ km s^{-1} (50% in model M1 and 95% for model M2), in good agreement with the value of *FWHM* = 440 km s^{-1} of RVPP02. The [S VIII] and [S IX] lines, with more than 50% emitted by clouds with $V_s < 300$ km s^{-1}, have large wings with $V_s = 1500$ km s^{-1}. Regarding the [Fe VII] line, it is better reproduced by model M2 than by model M1. In fact, model M2 shows that 60% of that line is emitted by clouds with $V_s = 300{-}500$ km s^{-1}, very close to the observed *FWHM* of 420 km s^{-1}. [Fe X] and [Fe XI] are another set of lines that deserves comments. Observationally, their line profiles have similar velocity distributions, with *FWHM* of 570 km s^{-1} and 695 km s^{-1}, respectively. This result must be compatible with the model outputs. In fact, model M1 predicts a large contribution (~60%) from high velocity clouds ($V_s \geq 500$ km s^{-1}) for both lines. In contrast, according to model M2, [Fe X] and [Fe XI] are mostly emitted by low velocity clouds with $V_s = 100$ km s^{-1} and 150 km s^{-1}. The contribution of high velocity clouds, in this case, is not larger than 30%.

In addition to the line broadening produced by the shock, bulk motions of the clouds around the gravitational potential of the central mass concentration should introduce an additional broadening, not taken into account in our modeling. Although a detailed calculation of the resulting profile is out of the scope of this paper, it is important to note that our results, overall, are consistent with the observed line widths. The reader should be aware that a complete modeling, able to simultaneously reproduce line fluxes and widths as well as local variations in most physical parameters, is not realistic because of the large number of free parameters, some of them unknown, that such an approach would require.

We conclude from the above discussion that model M1 is more representative of the actual conditions in the NLR of Ark 564 than model M2. In addition to better fit the observed line ratios, the predicted velocity distribution for the coronal gas is more consistent with the observations. The choice of model M1 is further reinforced by the discussion in the next section.

3.3. Relative contribution of the BLR emission

As it was pointed out in the Introduction Section, one of the main problems associated to the study of the NLR in NLS1 galaxies is the difficulty in obtaining a reliable estimate of the permitted lines fluxes emitted by that region. We recall here that the models calculated by SUMA refer to the NLR of Ark 564 because the code is not adapted to calculations for emission from a very dense gas. However, comparing the observed and calculated line ratios relative to Hβ, as is shown in Cols. 7 and 8 of Table 3 for models M1 and M2, respectively, allows us to derived roughly the contribution of the broad Hβ. This is possible because our permitted line flux measurements include the contribution from both the NLR and BLR while the predicted line ratios, relative to Hβ, do not include the broad line contribution. Thus, we expect that the calculated forbidden lines ratios, relative to Hβ, be higher than the observed ones.

This is in fact the situation found for the values predicted by model M1. They are ~1.3 higher relative to the ratios reported in Cols. 2 and 5 of Table 1, indicating that the predicted Hβ_{br} corresponds to about 70% of the total observed Hβ. On the other hand, for model M2 the values listed in Col. 8 of Table 3 indicate the opposite, suggesting that this model is unrealistic.

This result supports Rodríguez-Ardila et al. (2000) conclusions about the fraction of the NLR flux present in the observed Hβ line of NLS1 galaxies. They found that, on average, 50% of the total integrated Hβ flux is emitted by the NLR, in contrast to the fraction of 10% usually found in broad-line Seyfert 1 galaxies.

Notice that the ratio $(I_\lambda/\mathrm{H}\beta)_{\mathrm{calc}}/(I_\lambda/\mathrm{H}\beta)_{\mathrm{obs}}$ derived for He II λ4686/Hβ, He I λ5876/Hβ, is not constant, indicating that the broad contribution to He II λ4686, He I, and Hβ is different.

Finally, in Table 4 we compare the results of model calculations with the UV line ratios observed by Crenshaw et al. (2002), which include both the NLR and BLR contributions. Ratios less (higher) than unity indicate that the contribution of the BLR to the line is high (low).

Table 4. Ratio $(I_\lambda/\mathrm{H}\beta)_{\mathrm{calc}}/(I_\lambda/\mathrm{H}\beta)^1_{\mathrm{obs}}$ for the UV lines.

line	M1
Lyα	1.0
N v 1214	0.33
O iv]+Si iv λ1400	1.27
N iv] λ1486	0.50
C iv λ1550	1.23
He ii λ1640	4.7
O iii] λ1663	0.66
N iii] λ1750	0.22
Si iii] λ1890	1.60
C iii] λ1909	1.19
[Ne iv] λ2423	1.36
Mg ii λ2800	0.20

[1] From Crenshaw et al. (2002, Table 2, reddening corrected).

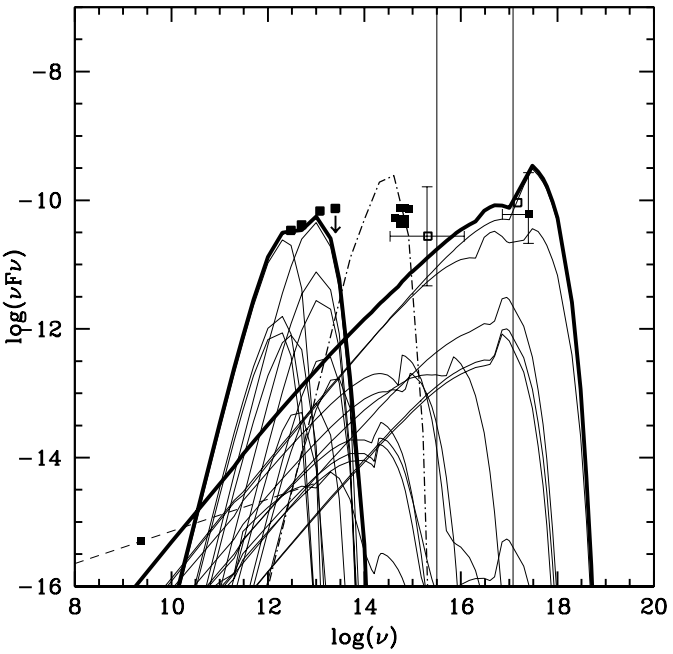

Fig. 1. The observed continuum of Ark 564 compared to the results of the multi-cloud model M1. The observed data from the NED are shown as filled squares. Open squares refer to the data of Walter & Fink (1993) in the X-ray and of Rodríguez-Pascual et al. (1997) in the UV. The multi-cloud emission, corresponding to dust emission and bremsstrahlung (thick solid lines) obtained from the weighted average of the clouds (thin solid lines) are shown, as well as the synchrotron emission from the shock front (dashed line). The old stellar population is represented by a blackbody (dot-dashed line). The frequency range where intrinsic absorption reduces the continuum flux is limited by the two thin vertical lines (see text).

4. The SED of the continuum

Following the results from the previous sections, model M1 is favored and its consistency with the observed continuum in a large range of wavelengths is checked below. In Fig. 1 the spectral energy distribution of the bremsstrahlung and of re-radiation by dust from model M1 is compared with the observed spectral energy distribution of Ark 564. The data were taken from De Vaucouleur et al. (1991); Zwicky & Kowal (1968); De Vaucouleurs & Longo (1988); Moshir et al. (1990) and Dressel & Condon (1978), compiled in the NED database. The datum in the soft X-ray range come from the *ROSAT* All Sky Survey, reported by Walter & Fink (1993) and the observed flux at 1450 Å comes from *IUE* observations of Rodríguez-Pascual et al. (1997).

Although the observed SED was constructed from data obtained at very different epochs, it should be representative thanks to the limited variability displayed by Ark 564 (Romano et al. 2002).

The most important physical mechanisms that should contribute to the emission of the continuum in the different frequency ranges are *(1)* bremsstrahlung from the photoionized gas ($\nu \sim 5\times10^{13}$–5×10^{15} Hz), *(2)* bremsstrahlung from the hot gas in the downstream region of shocked clouds ($\nu > 10^{16}$ Hz), *(3)* emission from the old star population ($\nu \sim 5\times10^{13}$–10^{15} Hz), *(4)* dust re-radiation in the infrared range ($\nu \sim 10^{12}$–10^{14} Hz), and *(5)* radio emission ($\nu < 10^{11}$ Hz).

Besides the line and continuum spectra, the SUMA code calculates re-radiation by dust in a consistent way. Dust is heated by the nuclear radiation flux; moreover, gas and dust mutually heat each other by collisions in shock turbulent regimes (Viegas & Contini 1994). Therefore, the frequency corresponding to the dust re-radiation peak depends on the shock velocity. At high V_s the grains will reach high temperatures in the post shock region and dust re-radiation will peak in the mid-IR, while at low velocities the peak appears in the far-IR. The peak intensity depends on the dust-to-gas ratio. Sputtering of the grains, which depends on the shock velocity, is calculated throughout the clouds. Small grains are rapidly sputtered. Therefore, we adopt silicate grains with an initial radius of 0.2 μm.

Line and continuum spectra must be modeled consistently. The single-cloud models are calculated assuming a standard dust-to-grain, by number, $d/g = 10^{-15}$, providing a first fit to the emission lines. Once the best fit is reached with a multi-cloud model, the continuum emission is checked and the d/g values for the single-clouds may change. In this case, an iterative process is carried out, in order to obtain a self-consistent model accounting for the observed emission-line and continuum data. Notice that an increase of d/g in the postshock region, before complete sputtering of the grains, acts as an increased density, speeding up the cooling processes. However, an increase by a factor less than 50 changes the cloud continuum emission without affecting the emission-line intensities.

The relative weights adopted to calculate the continuum SED are the same as those used to model the line spectra. The dust-to-gas ratios (by number) that fit the dust re-radiation fluxes in the IR appear in Table 2. At high V_s (models m13 and m14) the grains are completely sputtered at the shock front and we cannot determine the d/g ratio. The dust-to-gas ratio, by number, is $<10^{-13}$ in low velocity clouds and as high as 8×10^{-13} in clouds with $V_s = 500$ km s^{-1}. Recall that 10^{-14} by number corresponds to 4×10^{-4} by mass adopting silicate

grains with a density of 3 gr cm^{-3}. It means that in Ark 564 some high velocity clouds have dust-to-gas ratios higher than values found in the Galaxy. The high d/g found for some models (see Table 2) agrees to the relatively high $E(B-V)$ considered by Crenshaw et al. (2002). They claim, in fact, that the continuum spectrum of Ark 564 is clearly much flatter than that of Mrk 493 in the UV. This suggests that the spectrum of Ark 564 may experience a significant amount of internal reddening, which is supported by the Hα/Hβ = 3.4 measured by E97 and the small ratio of UV to X-ray continuum flux observed in Ark 564 compared to most Seyfert 1s (normal and NLS1s).

The two thin vertical lines in Fig. 1 show the range of frequencies corresponding to strong absorption in the UV (see Contini et al. 2002a), Within this interval, intrinsic absorption reduces the fluxes. Notice, for instance, that the hydrogen column density is $>10^{22}$ cm^{-2} for model m14. The data at $\nu \leq 10^{15}$ Hz show that contribution from the old stellar population is present in Ark 564 (dash-dot line), as is found for most AGN. In the radio band, only one measurement in one frequency is available, so we cannot decide whether there is also some contribution from synchrotron emission created by Fermi mechanism at the shock front (dashed line, see Contini & Viegas 1999).

5. Discussion

The models which could better fit the coronal lines of NLS1 galaxies, including Ark 564, were already discussed in RVPP02 and they are based on line ratios extracted from a general grid of composite models (Contini & Viegas 2001). The asymmetries toward the blue observed in the line profiles of Ark 564 (E97) suggest that these lines originate in a gas outflowing from the nucleus, supporting the models that combine the effect of shocks and photoionization. That first approach was a start for a more detailed analysis of the NLR of these objects, as presented in this paper. Here, emission-lines in a large range of wavelengths and ionization levels constrain the modeling and reveal that many different conditions coexist in the NLR. Notice that multi-cloud models were used previously in the detailed modeling of NGC 5252, Circinus, NGC 4151, and NGC 7130 (Contini et al. 1998a,b, 2002a,b).

The multi-cloud models in Ark 564 show three main types of cloud velocities: (a) those between 100 and 150 km s^{-1}, which are about the lowest observed in AGN and are typical of LINERS. Very low velocities clouds, with $V_s \sim 60$ km s^{-1}, have been found to contribute only to the spectra of Circinus; (b) velocities of about 300−500 km s^{-1}, generally present in the NLR; (c) high-velocity clouds ($\geq$1000 km s^{-1}), also invoked in modeling the Seyfert galaxies referred above, have been used in order to explain high ionization lines (e.g. [Fe X]) as well as the soft X-ray emission. In the high-V_s clouds the d/g ratios are higher than in lower-velocity clouds by a factor of ∼100 both in Circinus and in NGC 4151. High-velocity shocks lead to a strong heating of gas and dust. However, the upper limit shown by Ark 564 in the NIR continuum at log $\nu = 13.5$ constrains the d/g in the high-velocity clouds to lower values. The same conclusion was obtained for NGC 5252.

Preshock densities $n_0 \leq 1000$ cm^{-3} are found in Ark 564, as well as in the other previously modeled galaxies. Only in the warm absorber of NGC 4051, another NLS1, preshock densities up to 10^6 cm^{-3} were found in clouds characterized by very small D ($\geq 2 \times 10^{12}$ cm).

Although the models for Ark 564 were chosen among those that better fit the strongest lines, they should be able to reproduce as many lines as possible. We briefly show the complex modeling of such a rich spectrum, discussing for instance [Si X]/[Si VI] relative to [Fe XI]/[Fe X] line ratios. The observations show that [Si X]/[Si VI] ≥ 2 and [Fe XI]/[Fe X] > 1. Model m6, which is matter-bounded and RD, gives the right trend for the Fe lines but strongly underestimates the [Si VI]/Hβ line ratio, which is otherwise high in models composed of clouds with large D. In order to get a consistent picture, the models must be summed up with a fine tuning of the relative weights in order to reach an agreement between observed and calculated ratios for all the lines.

Finally, if the NLR spectrum of Ark 564 is well reproduced by composite models accounting for the effect of photoionization by a central source and shocks, it is then natural to ask about the origin of such shocks. Although SUMA does not discriminate about the shock sources, the fact that Ark 564 has an extended radio emission makes jet-induced shocks a likely scenario. This hypothesis is particularly suitable to explain the low-ionization lines. High-velocity shocks, found to be adequate for coronal lines, may have their origin from outflowing material that evaporates from the torus. This last hypothesis, in fact, was already considered by E97 and RVPP02 from their observations of coronal lines. In summary, the broad range of shock velocities found from our modeling is consistent with shocks generated, at least, from two distinct mechanisms.

6. Concluding remarks

In the previous sections we have modeled, in detail, the observed continuum and line emission spectrum of the NLS1 galaxy Ark 564. Particular emphasis is put on the constrains imposed by the coronal lines. This is the first time that such an approach is carried out for the NLR of a NLS1 galaxy. The line spectrum ranges from UV to NIR wavelengths while the continuum extends from radio to X-ray. Composite models accounting for the combined effect of photoionization by a central source plus shocks are used to that purpose. We found a multi-cloud model that can suitably reproduce most of the observed line ratios within a factor of 2 and yields shock velocities consistent with the observed line widths. The picture that emerges from our modeling is a NLR composed of cloud showing a large range of velocities (V_s = 100−1500 km s^{-1}), preshock densities (n_0 = 100−700 cm^{-3}) and illuminated by different flux intensities, from 0 in SD models to $F_H = 5 \times 10^{12}$ photons cm^{-2} s^{-1} eV^{-1} at 1 Ryd in RD models. The cloud geometrical thickness D was found to be between 3 and 10 pc, but some of them represent filaments with $D < 1$ pc. The single-cloud models are summed up adopting relative weights. The best fitting model (M1) is obtained by adopting the highest weights for SD clouds with $V_s = 150$ and high velocity-density RD clouds reached by a strong radiation flux. These high

velocity clouds, particularly SD clouds with $V_s = 1500$ km s^{-1} account for the soft X-ray emission and for most of the flux from the [Fe X], [Fe XI], and [Fe XIII] lines (70%, 60%, and 55%, respectively). Clouds with $V_s = 150$ km s^{-1} and $n_0 = 600$ cm^{-3}, illuminated by the strong central continuum flux, also contribute to the coronal lines. On the other hand, low ionization lines in the optical range are mostly emitted from SD clouds. In the modeling process we have considered forbidden line intensities relative to [O III], in order to avoid the broad line contribution that is present in the permitted lines.

The input continuum energy distribution in the UV–X-ray region that photoionizes the NLR of Ark 564 is characterized by a spectral index $\alpha = -1.5$. This value is very close to the α measured from UV and X-rays observations. That means that the NLR of Ark 564 is directly illuminated by the radiation of the central source. In addition, shocks, probably originated from outflowing material that evaporates from the torus, provide an additional input mechanism for the production of coronal lines.

To complete the modeling, we have roughly evaluated the contribution of the BLR to the total Hβ line and to the permitted lines in the UV. A quantitative calculation is not possible because the SUMA code is not adapted to the calculation of lines from high density gas. However, it is found that H$\beta_{\rm broad}$/H$\beta_{\rm narrow}$ should range between 1 and 2, in very good agreement with the value found by Rodríguez-Ardila et al. (2000) for NLS1 galaxies and determined from Gaussian fitting to the observed permitted profiles.

Finally, we could consistently explain the data of the continuum by the multi-cloud model M1. A gas-to-dust ratio between 10^{-15} and 10^{-12} by number has been found for the NLR clouds, showing different values in different clouds.

Acknowledgements. We are very grateful to the referee, Dr. P. Ferruit, for many interesting comments which improved the presentation of the paper. This paper is partially supported by the Brazilian agencies FAPESP(00/06695-0) and CNPq (304077/77-1). This research has made use of the NASA/IPAC extragalactic database (NED), which is operated by the Jet Propulsion Laboratory, California Institute of Technology, under contract with the National Aeronautics and Space Administration.

References

Allen, C. W. 1973, in Astrophysical Quantities (Athlon Press)
Allen, D. A. 1979, MNRAS, 186, 1
Boller, Th., Brandt, W. N., & Fink, H. 1996, A&A, 305, 53
Boroson, T. A., & Green, R. F. 1992, ApJS, 80, 109
Collier, S., Crenshaw, D. M., Peterson, B. M., et al. 2001, ApJ, 561, 146
Constantin, A., & Shields, J. C. 2003, PASP, 115, 592
Contini, M., Prieto, M. A., & Viegas, S. M. 1998a, ApJ, 492, 511
Contini, M., Prieto, M. A., & Viegas, S. M. 1998b, ApJ, 505, 621
Contini, M., & Viegas, S. M. 1999, ApJ, 523, 114
Contini, M., & Viegas, S. M. 2000, ApJ, 535, 721
Contini, M., & Viegas, S. M. 2001, ApJS, 132, 211
Contini, M., Viegas, S. M., & Prieto, M. A. 2002a, A&A, 386, 399
Contini, M., Radovich, M., Rafanelli, P., & Richter, G. M. 2002b, ApJ, 572, 124
Crenshaw, D. M., Kraemer, S. B., Turner, T. J., et al. 2002, ApJ, 566, 187
De Vaucoleurs, A., & Longo, G. 1988, in the Catalogue of Visual and Infrared Photometry gor Galaxies from 0.5 to 10 micrometer (1961–1985), University of Texas Monographs in Astronomy (Austin: University of Texas)
De Vaucouleurs, G., De Vaucouleurs, A., Corwin, H. G. Jr., et al. 1991, in Third Reference Catalogue of Bright Galaxies (New York: Springer-Verlag)
De Robertis, M. M., & Osterbrock, D. E. 1984, ApJ, 286, 171
Dressel, L. L., & Condon, J. J. 1978, ApJ, 36, 53
Erkens, U., Apenzeller, I., & Wagner, S. 1997, A&A, 323, 707 (E97)
Ferguson, J. W., Korista, K. T., & Ferland, G. J. 1997, ApJS, 110, 287
Goodrich, R. W. 1989, ApJ, 342, 224
Leighly, K. M. 1999, ApJS, 125, 297
Moran, E. C. 2000, New Astron. Rev., 44, 527
Moshir, K., Kopan, G., Conrow, T., et al. 1990, BAAS, 22, 1325
Nagao, T., Murayama, T., & Taniguchi, Y. 2001, ApJ, 546, 744
Oliva, E., Salvati, M., Moorwood, A. F. M., & Marconi, A. 1994, A&A, 288, 457
Osterbrock, D. E., & Pogge, R. W. 1985, ApJ, 297, 166
Penston, M. V., Fosbury, R. A., Boksenberg, A., Ward, M. J., & Wilson, A. S. 1984, MNRAS, 208, 347
Peterson, B. M., & Wandel, A. 2000, ApJ, 540, L13
Rodríguez-Ardila, A., Pastoriza, M. G., Binette, L., & Donzelli, C. J. 2000, ApJ, 538, 581
Rodríguez-Ardila, A., Viegas, S. M., Pastoriza, M. G., & Prato, L. 2002, ApJ, 579, 214 (RVPP02)
Rodríguez-Pascual, P. M., Mas-Hesse, J. M., & Santos-Lleo, M. 1997, A&A, 327, 72
Romano, P., Mathur, S., Pogge, R. W., Peterson, B. M., & Kuraszkiewicz, J. 2002, ApJ, 578, 64
Shemmer, O., Romano, P., Bertram, R., et al. 2001, ApJ, 561, 162
Turner, T. J., Romano, P., George, I. M., et al. 2001, ApJ, 561, 131
Veilleux, S. 1988, AJ, 95, 1695
Viegas, S. M., & Contini, M. 1994, ApJ, 428, 113
Viegas-Aldrovandi, S. M., & Contini, M. 1989, A&A, 216, 253
Walter, R., & Fink, H. H. 1993, A&A, 274, 105
Zwicky, F., & Kowal, C. T. 1968, in the Catalogue of Galaxies and of Clusters of galaxies, vol. VI (Pasadena: California Institute of Technology)